Pop-Up Detector Test Report

Version 1.0 -- 2 May 2000

C. Darren Dowell
Caltech, Mail Code 320-47
Pasadena, CA 91125
(626)395-6610 (office)
(626)395-2600 (lab)
(626)796-8806 (FAX)
cdd@submm.caltech.edu

Abstract

Measurements of semiconducting pop-up bolometers were performed at Caltech in April 2000. We report the resistance vs. temperature and the thermal characteristics of the measured samples. The desired SHARCII and HAWC parameters were bracketed with the measured samples, and we make recommendations for the bolometer designs for the two instruments.

Acknowledgments

Walter Collins (Caltech), Mino Freund (Goddard), Matt Gardner (Caltech), and Jeff Groseth (Caltech) helped considerably with preparing the test components and in performing the measurements. Attila Kovacs (Caltech) wrote the software to solve for bolometer parameters from measured data. Christine Allen (Goddard) provided the bolometer samples and advice for handling them. Harvey Moseley (Goddard) provided guidance through the testing period. This research was funded in part by NSF grant AST 9615025 to the Caltech Submillimeter Observatory.

Outline

Measurement Apparatus

Implant and bolometer samples were tested in the SHARCII cryostat, which contains a ^{3}He refrigerator enclosed in a L^{4}He-cooled radiation shield. For most measurements, the main L^{4}He reservoir was pumped down to 1.5 K so that the device substrate reached temperatures as low as 0.325 K.

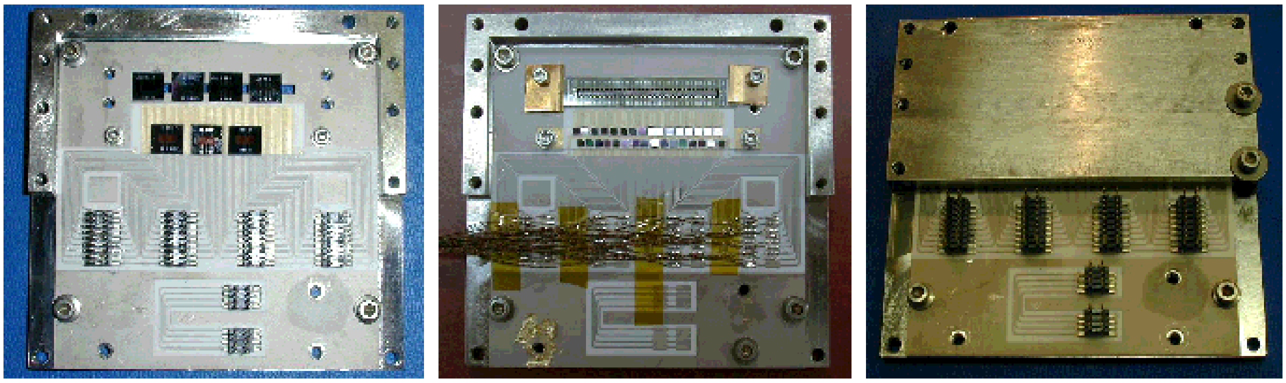

Figure 1. Caltech interface substrate (alumina). The 3-element implant screening devices were GE varnished to the substrate, and the 32-element bolometer arrays were clipped to the substrate. Gold wedge bonds provided electrical connection between the devices, load resistors, and substrate. Surface-mount connectors were initially used to interface with the cryostat wiring. However, they were replaced with directly soldered wires for later measurements. The ceramic substrate was enclosed in an INVAR box. A sheet of gold leaf and the force of ~6 screws were used to thermally connect the INVAR and ceramic.

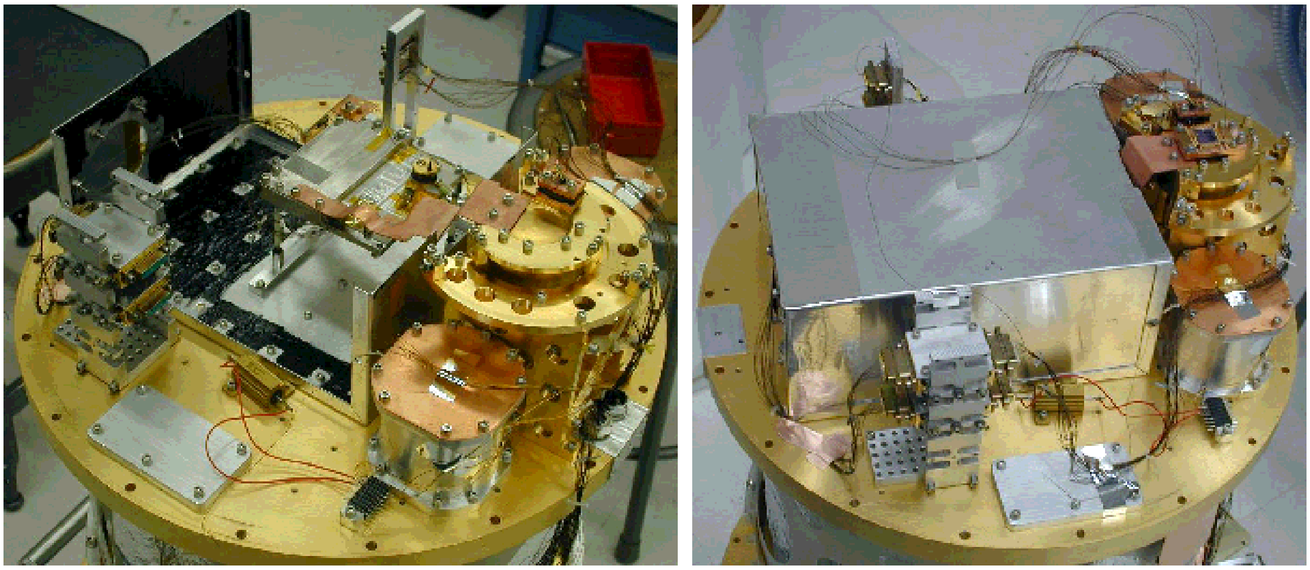

Figure 2. Device suspension and shielding. The ceramic/ INVAR package was suspended from the L^{4}He coldplate with 3-4 fiberglass tubes with A/L = 0.014-0.018 cm. The package was heat sunk to the fridge through an annealed OFHC copper strap with A/L = 0.014 cm. A calibrated LakeShore GRT was attached to the ceramic substrate with a screw and gold leaf, approximately 5 cm from the detectors. The package was shielded by a secondary L^{4}He enclosure with blackened walls. With this configuration, the coldest observed GRT measurement for the detector package was 0.325 K, during which the L^{4}He bath

was at 1.5 K, the fridge was at 0.291 K, and the extrapolated parasitic heat load on the detector package was 2-4 microW. The JFET modules were located outside the inner shield.

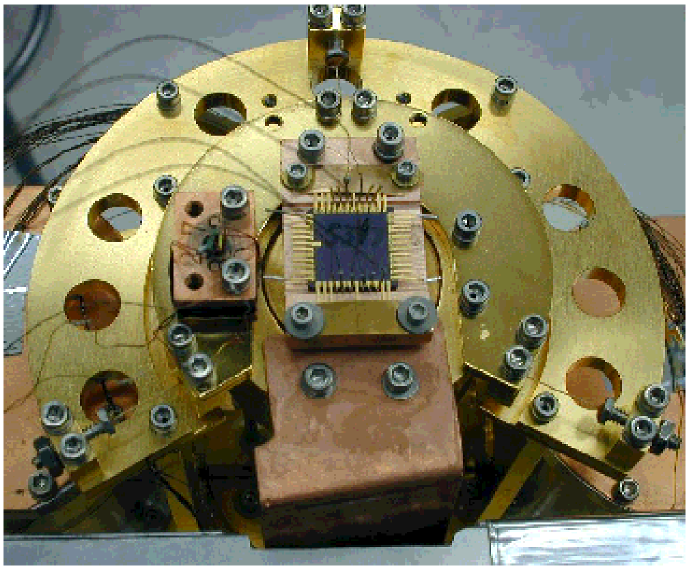

Figure 3. Additional implant screening hardware. In order to confirm the implant resistances, the 3-element devices in the Goddard-selected ceramic package were clipped to a copper block and installed directly on the SHARC II fridge coldhead or in a separate L^4He cryostat (the purple 'Barney' Dewar).

All wires going into the Dewar pass through one or two RFI-filtered connectors, which contain 4 nF capacitors from each pin to the Dewar wall.

Thermal Performance of Detector Package

The silicon frame has a thickness of 300 microns. In the direction of heat flow from bolometer 1 to bolometer 32, the relevant A/L is 0.0035 cm. For a 0.3 K thermal conductivity of XXX...

The wirebonds were 0.001 inch diameter 99.99% gold. With 64 each 3 mm long wire bonds (total A/L=0.001 cm), and assuming a 0.3 K thermal conductivity of 0.1 W/cm/K (Touloukian et al. 1970), the effective G of the wirebonds was 100 microW/K. We have ignored unknown boundary thermal resistance, which will reduce the effective G.

The ceramic substrate is approximately 7 cm x 7 cm x 0.06 cm, giving an A/L of 800 cm in the thickness (shortest) direction. Assuming a 0.3 K thermal conductivity of 11 microW/cm/K (Locatelli et al. 1976), the thermal conductance from the INVAR enclosure to the trace side of the ceramic board is G = 9000 microW/K. Again, we have ignored boundary thermal resistance.

The heat strap also limits the cooling of the detector wafer. During the cooldowns reported here, the fridge/heat strap combination was observed to have an effective G of 80 microW/K at the coldest temperatures.

Combining the effective G's of the wire bonds, ceramic board, and heat strap, we estimate an effective G of 40 microW/K for the link from the silicon die to the ^3He fridge, three orders of magnitude greater than the G of the membrane devices. For a maximum 0.5 V bias across the 64 each 30 Mohm load resistors and detectors, the dissipated power can be at most 0.5 microW, leading to a temperature rise of at most 13 mK. For the 0.5 V bias, the detector package was observed to slowly warm a few mK. However, the measurements with the 0.5 V bias were performed quickly, using the thermal inertia of the detector package to keep the detector cool.

Designs of Test Bolometers

Three types of bolometer arrays were manufactured for the detector measurements:

- 3-element implant screening dies with all membrane (high G) devices
- 32-element G_0 variety packs with a range of thermal designs (HGUNITs)
- 32-element thermistor variety packs with a range of thermistor designs (THUNITs)

The metallization of the measured wafers was aluminum.

HAWC Calibration Run   Detector Statistics   Code 553

Cell Name	Torsion Bar Width	Torsion Bar Length	Radius of Curvature	Strap Width	Strap Length	Metal on Torsion Bar	Added Metal on Strap	Implant LxW	Location on array	Optimized LxW target
Membrane device	NA	NA	NA	NA	NA	Lots	Lots	940x650	1, 32	
HGUNIT.1A	10	456	40	295	500	10	10 wide leads (4	940x650	29, 30, 31	940 x 650 Ratio 1.44
HGUNIT.2A	16	421	70	295	500	16	16 wide leads (4	940x650	26, 27, 28	
HGUNIT.2B	16	421	70	295	500	na	16 wide leads (4	940x650	23, 24, 25	
HGUNIT.2C	16	421	70	295	500	na	16 wide leads (4 ea), 100 wide strap	940x650	20, 21, 22	
HGUNIT.2D	16	421	70	295	500	16	16 wide leads (4 ea), 100 wide strap	940x650	17, 18, 19	
HGUNIT.3A	40	590	100	290	310	40 wide, 1/2 length of torsion	40 wide leads, (4 ea)	940x650	14, 15, 16	
HGUNIT.3B	40	590	100	290	310	40 wide, length of torsion bar	40 wide leads, (4 ea)	940x650	11, 12, 13	
HGUNIT.3C	40	590	100	290	310	na	40 wide leads (4 ea), 100 wide strap	940x650	8, 9, 10	
HGUNIT.3D	40	590	100	290	310	40 wide, length of torsion bar	40 wide leads, (4 ea), 100 wide strap (2 ea)	940x650	5, 6, 7	

Prepared by Christine Allen 4/12/00   Page 1

Table 1. Recipes for bolometers on G_0 test arrays.

Cell Name	Torsion Bar Width	Torsion Bar Length	Radius of Curvature	Strap Width	Strap Length	Metal on Torsion Bar	Added Metal on Strap	Implant LxW	Location on array	Optimized LxW target
Membrane device	NA	NA	NA	NA	NA	Lots	Lots	940x650	1, 32	
UNIT.2B	16	421	70	295	500			940x650	6, 27, 28, 29, 30, 31	
THUNIT2B.1	16	421	70	295	500			900x990	5, 22, 23, 24, 25, 26	
THUNIT2B.2	16	421	70	295	500			230x160	4, 17, 18, 19, 20, 21	
THUNIT2B.3	16	421	70	295	500			460x320	3, 12, 13, 14, 15, 16	
THUNIT2B.4	16	421	70	295	500			120x80	2, 7, 8, 9, 10, 11	

Table 2. Recipes for bolometers on thermistor test arrays.

Wafer Number	Net Density
5347	0.75
5327	0.70
5168	0.70
5306	0.65
5250	0.60
5260	0.50

Table 3. Implant doses. Higher net density means greater implant dose, which means lower cold resistance. Wafers 5347 and 5327 are of interest for SHARCII and HAWC. (Wafer 5168 was not tested.)

Thermistor Screening Results

The first part of the detector measurement program was to screen five wafers for desired resistance at cold temperatures. Three-element membrane devices were measured in three configurations -- GE varnished to the Caltech ceramic interface board, packaged in the Goddard ceramic carrier on a copper block in the purple L^4He Dewar, and in the Goddard carrier/copper block on the SHARCII coldhead.

Resistance measurements were made with a Keithley 616 Digital Electrometer borrowed from Goddard that allows current excitations from 1 pA to 1 microA stepped by factors of 10. The reported measurements were made with the highest current setting which did not cause significant self heating. The criterion was to allow no more than a 2% effect on the observed resistance.

SHARCII Dewar, Large Ceramic Board

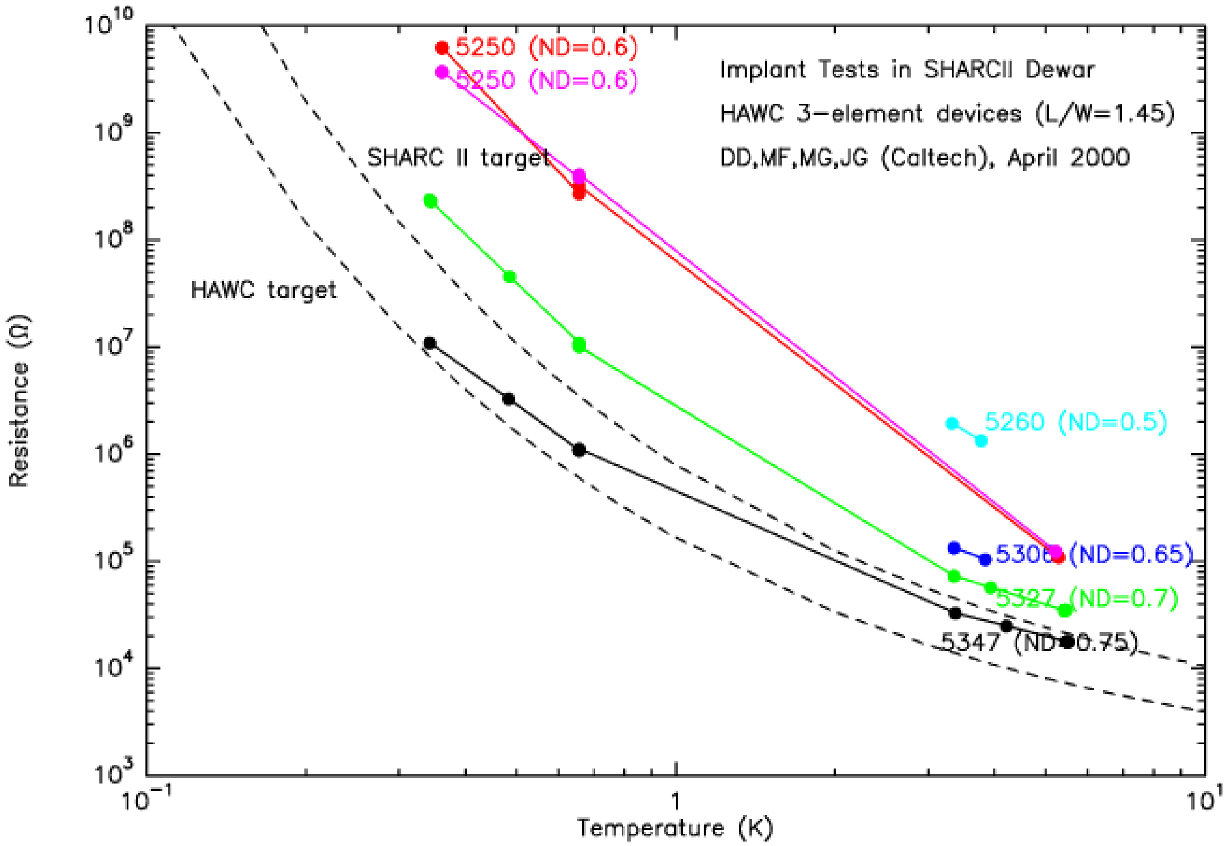

Figure 4. Resistance measurements for 3-element membrane devices on Caltech ceramic board. The SHARCII target curve is T_0 = 40 K, R_0 = 1430 ohm (Moseley et al. 1999), and the HAWC target is T_0 = 30 K, R_0 = 700 ohm (Moseley 1999).

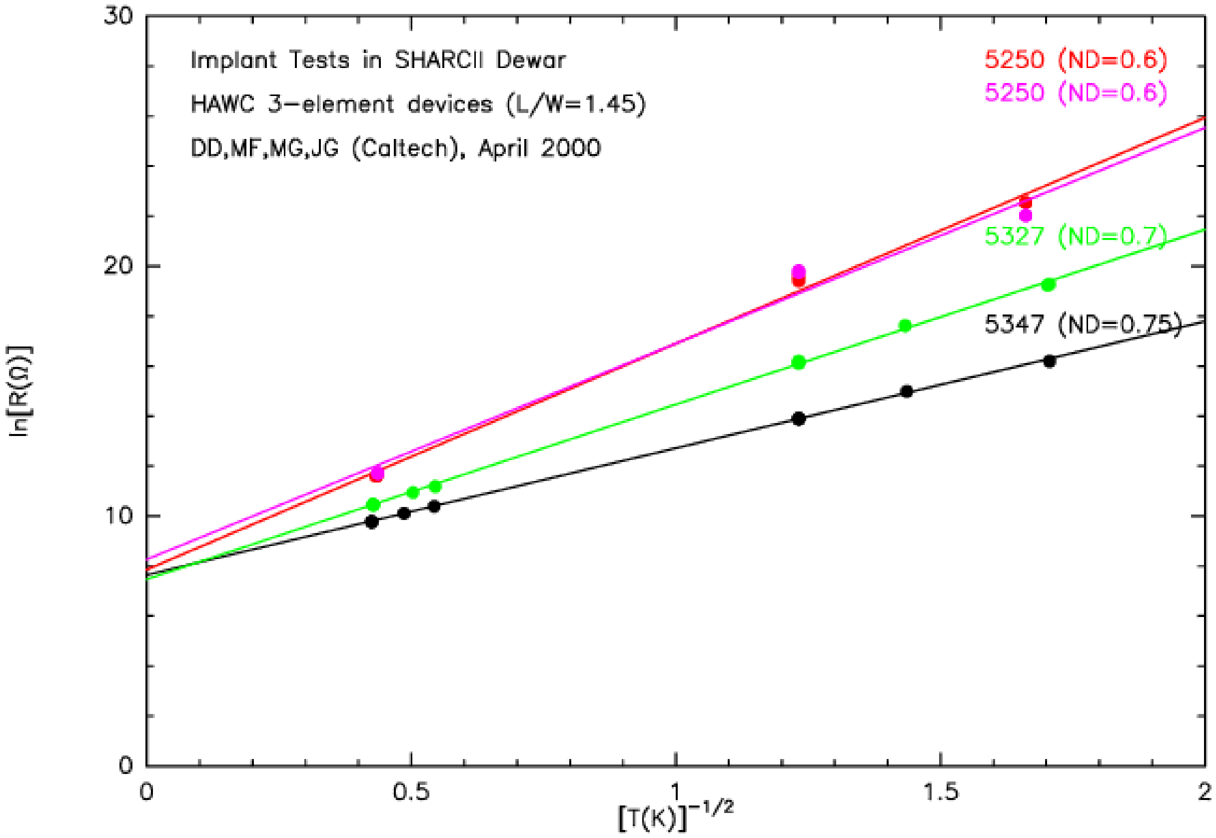

Figure 5. Resistance measurements plotted in units which give linear fits.

A fit to the data with model $R = R_0 \exp[(T_0/T)^{1/2}]$ yields:

Label	ND	R0 (ohms)	T0 (K)
5250a	0.6	2570	81.8
5250b	0.6	3880	74.6
5327	0.7	1750	48.9
5347	0.75	2090	25.7

Table 4. Fits for resitance of implant devices on Caltech ceramic board.

Purple Dewar, Small Ceramic Package

Three-element dies were tested using the Goddard-provided ceramic packages attached 'upside down' to a copper block in order to shield the devices from radiation. Resistances were measured with the Keithley 616 electrometer.

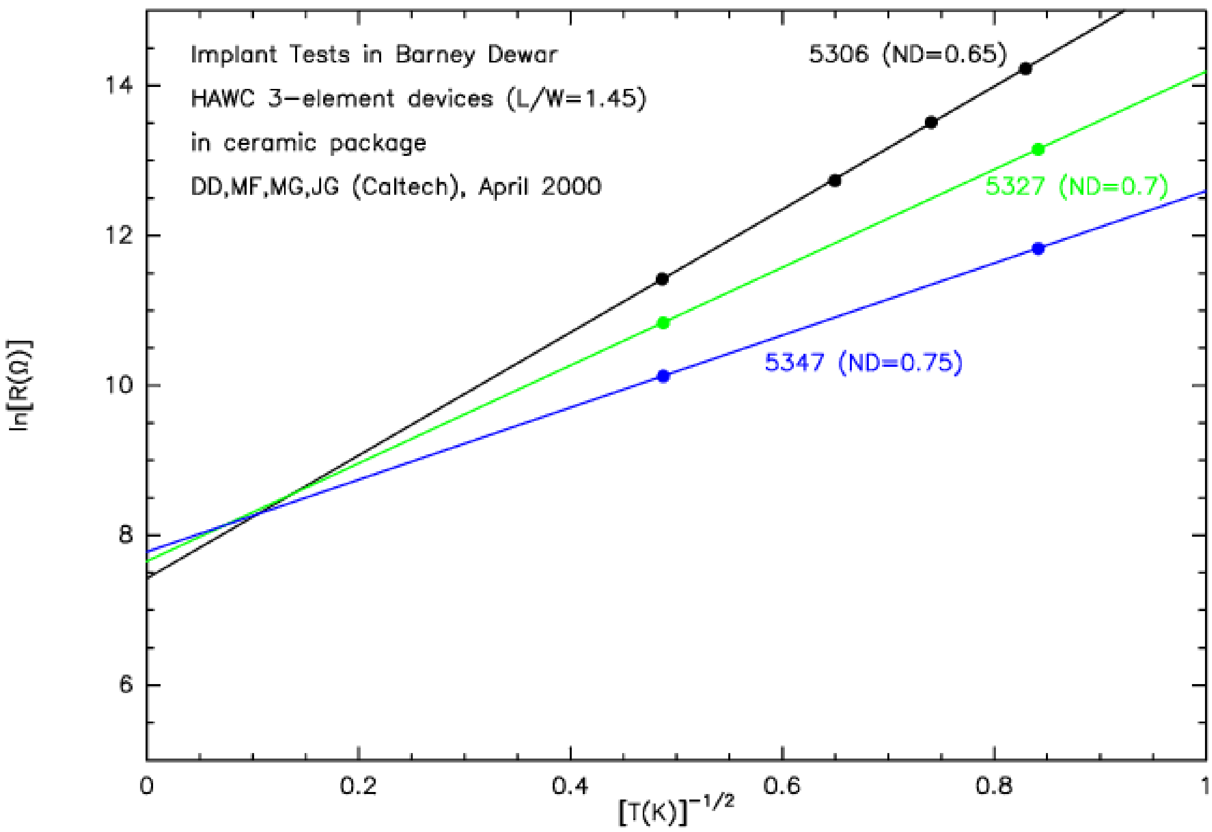

Figure 6. Measurements of thermistor samples in the purple Dewar.

A fit to the data from the purple Dewar experiment only yields:

Label	ND	R0 (ohms)	T0 (K)
5306	0.65	1670	67.3
5327	0.7	2100	42.7
5347	0.75	2380	23.2

Table 5. Purple Dewar thermistor fits.

SHARCII Dewar, Small Ceramic Package on Coldhead

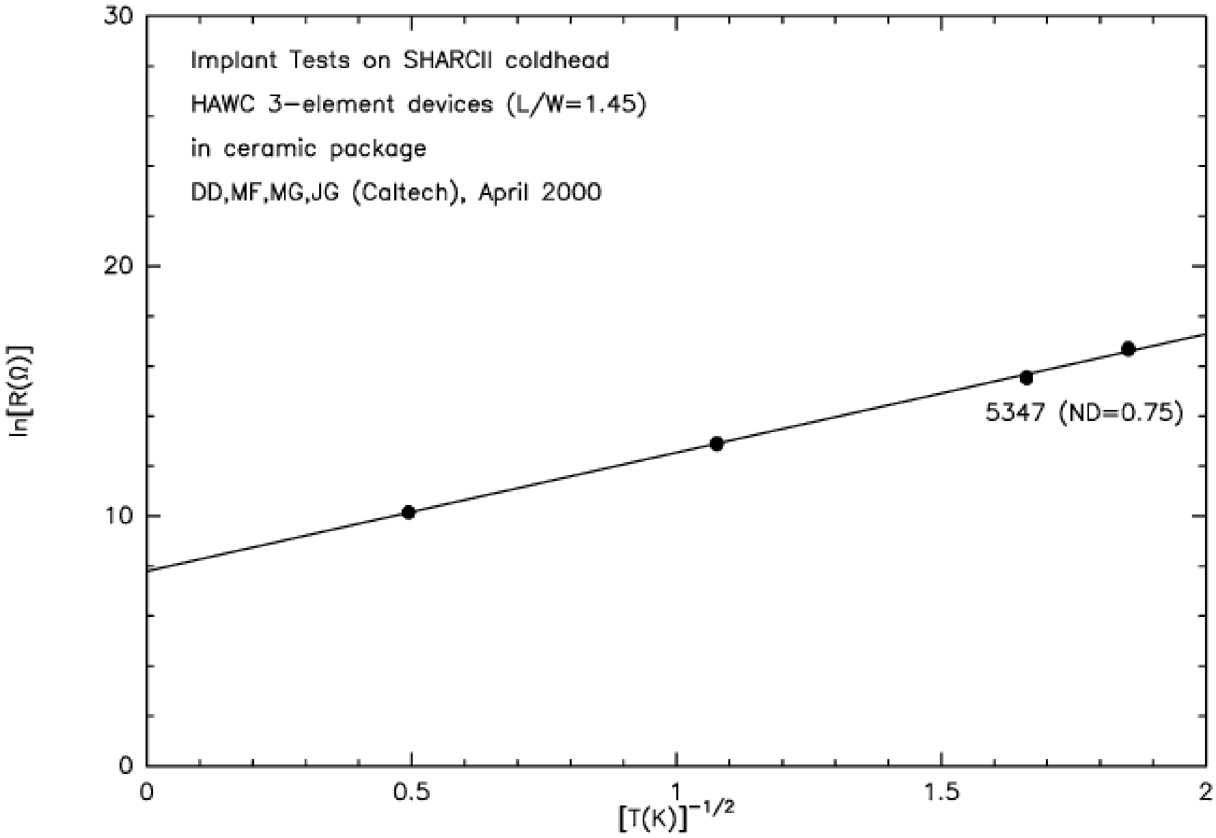

Figure 7. Measurements of thermistor sample on the SHARC II coldhead. The coldest measured temperature was 0.291 K.

Label	ND	R0 (ohms)	T0 (K)
5347	0.75	2430	22.5

Table 6. SHARCII coldhead thermistor fit.

Comparison of Samples

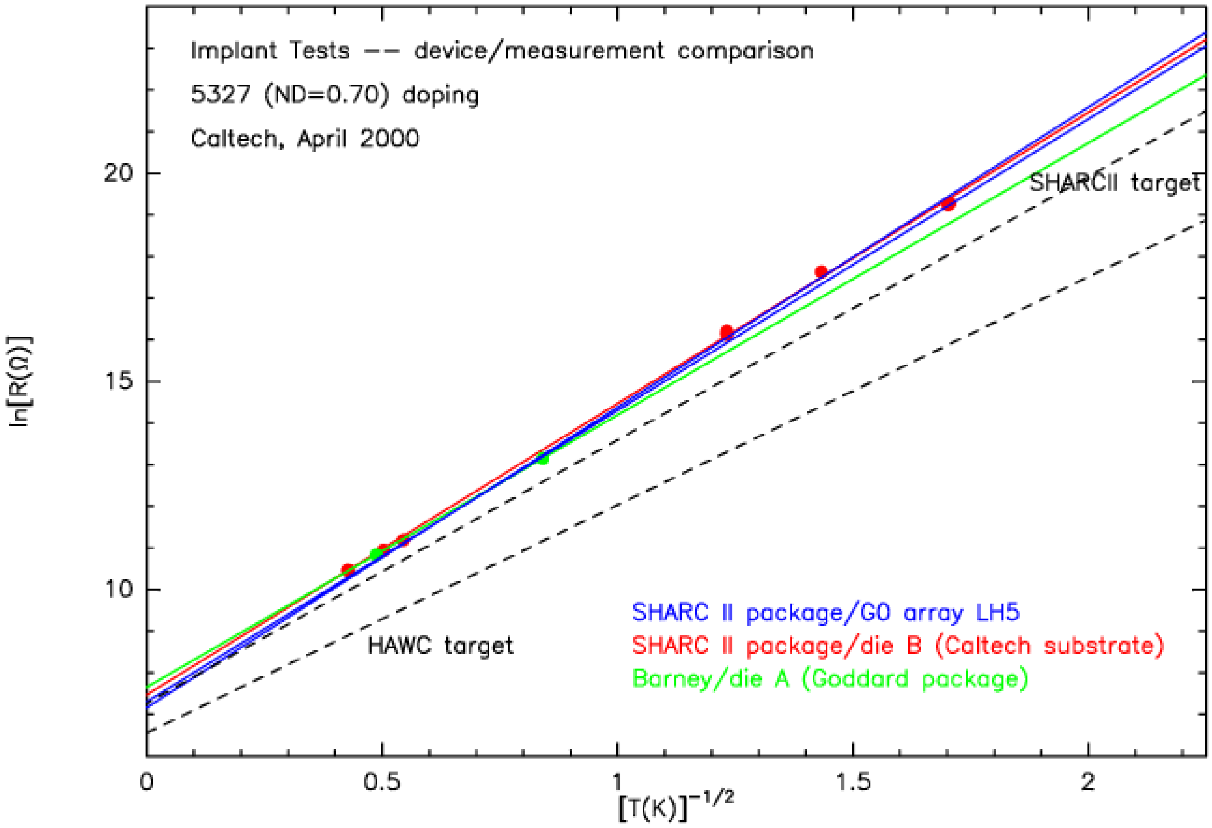

Figure 8. Measurements of 5327 thermistor samples. Two membrane dies and one 32-element bolometer array were measured. The fits for the bolometer array represent the extreme values for the array. There is reasonable agreement among the different samples. The resistance is too high for both HAWC and SHARCII.

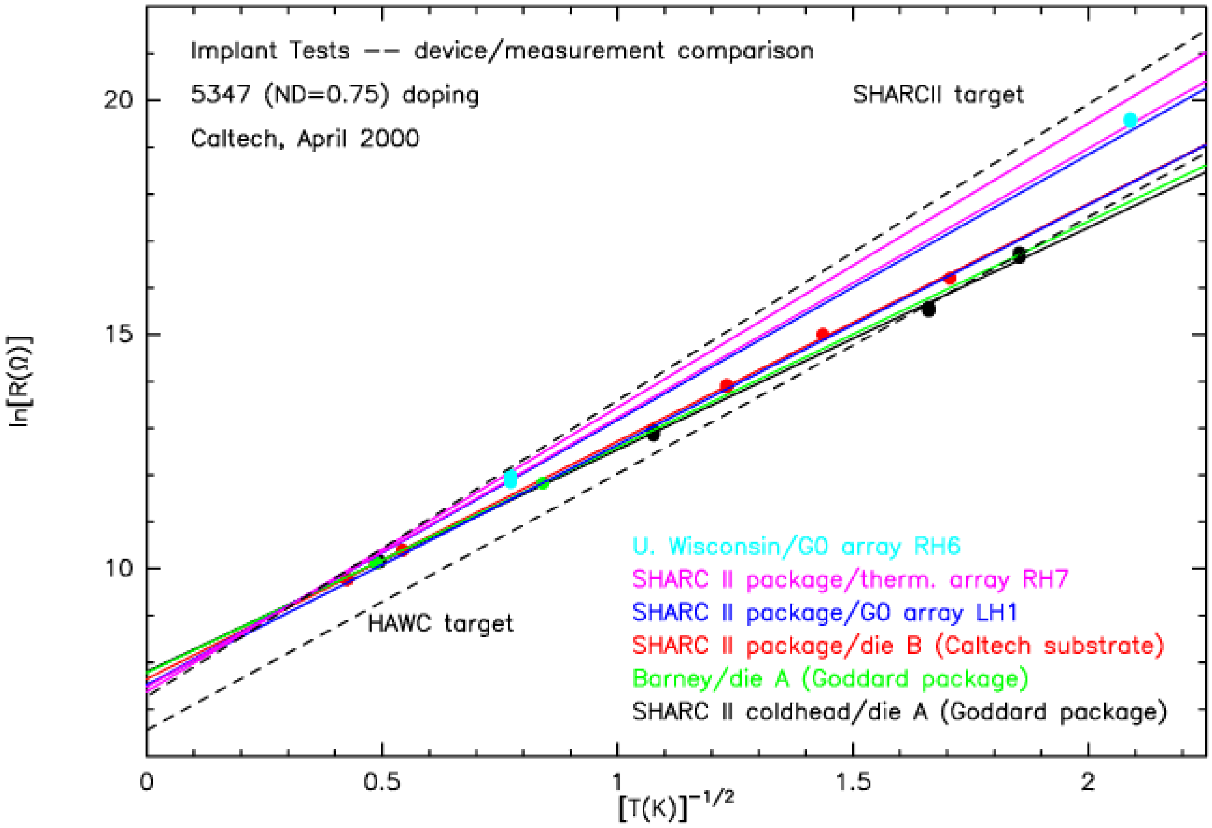

Figure 9. Measurements of 5347 thermistor samples. Two membrane dies and three 32-element arrays were measured. (The thermistor array measurements were normalized to L/W = 1.45.) There is considerable variation from sample to sample, which nearly covers the range from the HAWC target to the SHARC II target. There is good agreement between the measurements for membrane die A in the purple Dewar (green curve) and SHARC II (black curve).

Results for 5327 G_0 Test Array LH5

For tests of G_0 array 5327 LH5 (ND=0.7), the silicon frame was clipped to the detector board with beryllium-copper clips and gold wedge bonded. Bolometers 17-29 and 32 were wired in series with 150 Mohm SiCr load resistors from MSI. The resistance of a SiCr load varies with temperature (up to 210 Mohms at 0.33 K); this effect was measured for a few resistors and modeled for all of them in the analysis.

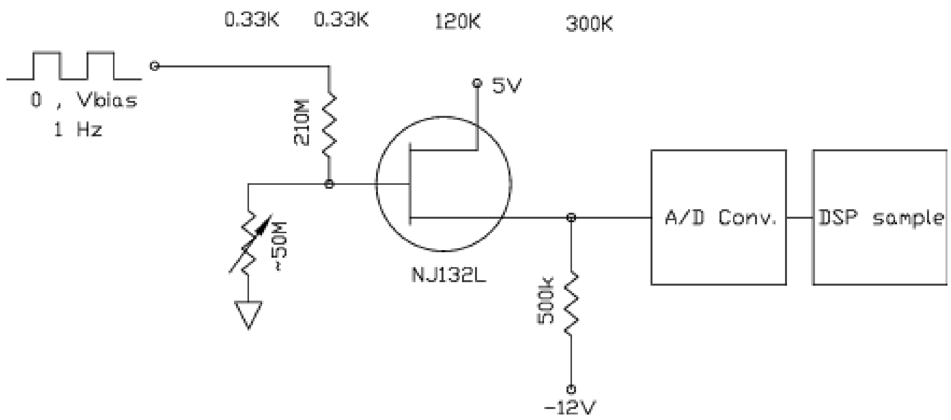

Figure 10. Circuit used to measure IV curves. 16 JFETs were available, so up to 16 bolometers were measured simultaneously. The JFET gain was approximately 0.996. The bias voltage was slowly stepped from 0 V to a nonzero value. The change in voltage from the JFET gives the bolometer voltage, which yields the bolometer resistance since the load resistance is known (to 5% accuracy).

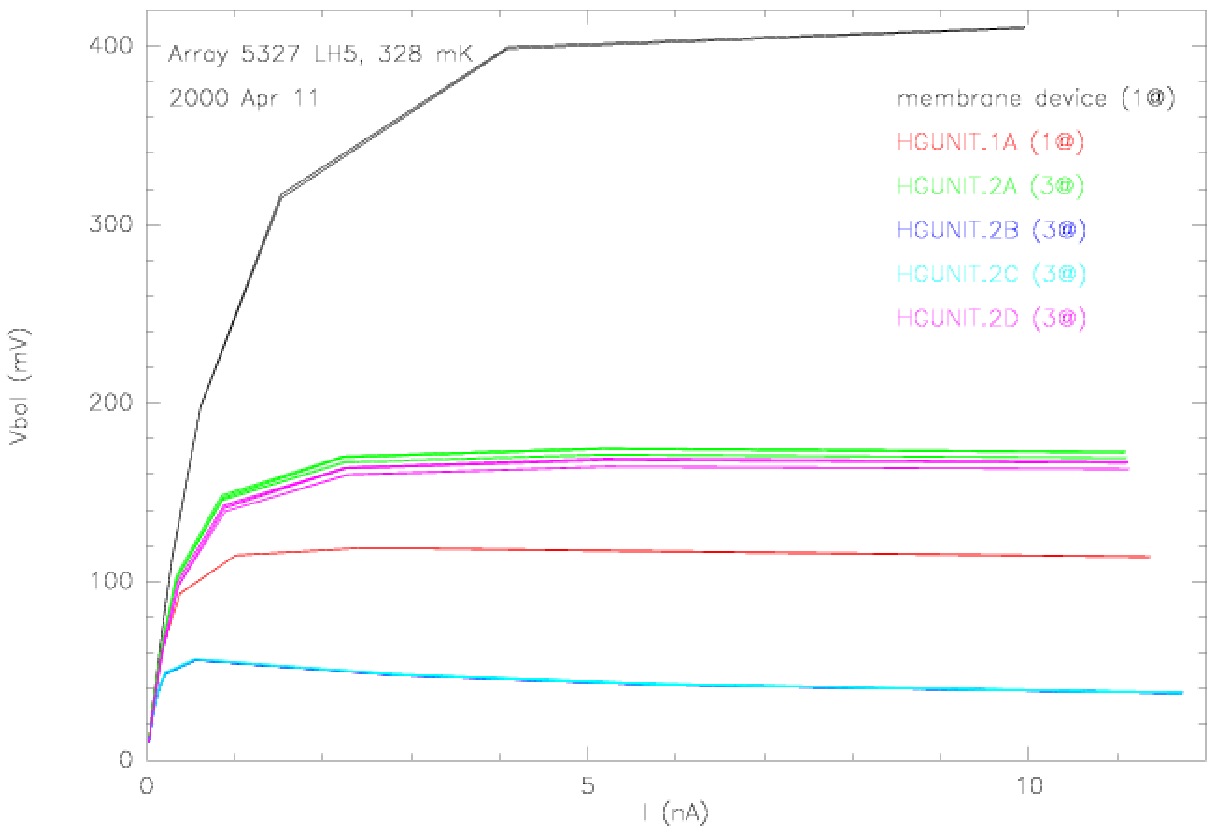

Figure 11. Sample IV curves for all bolometers at a single temperature.

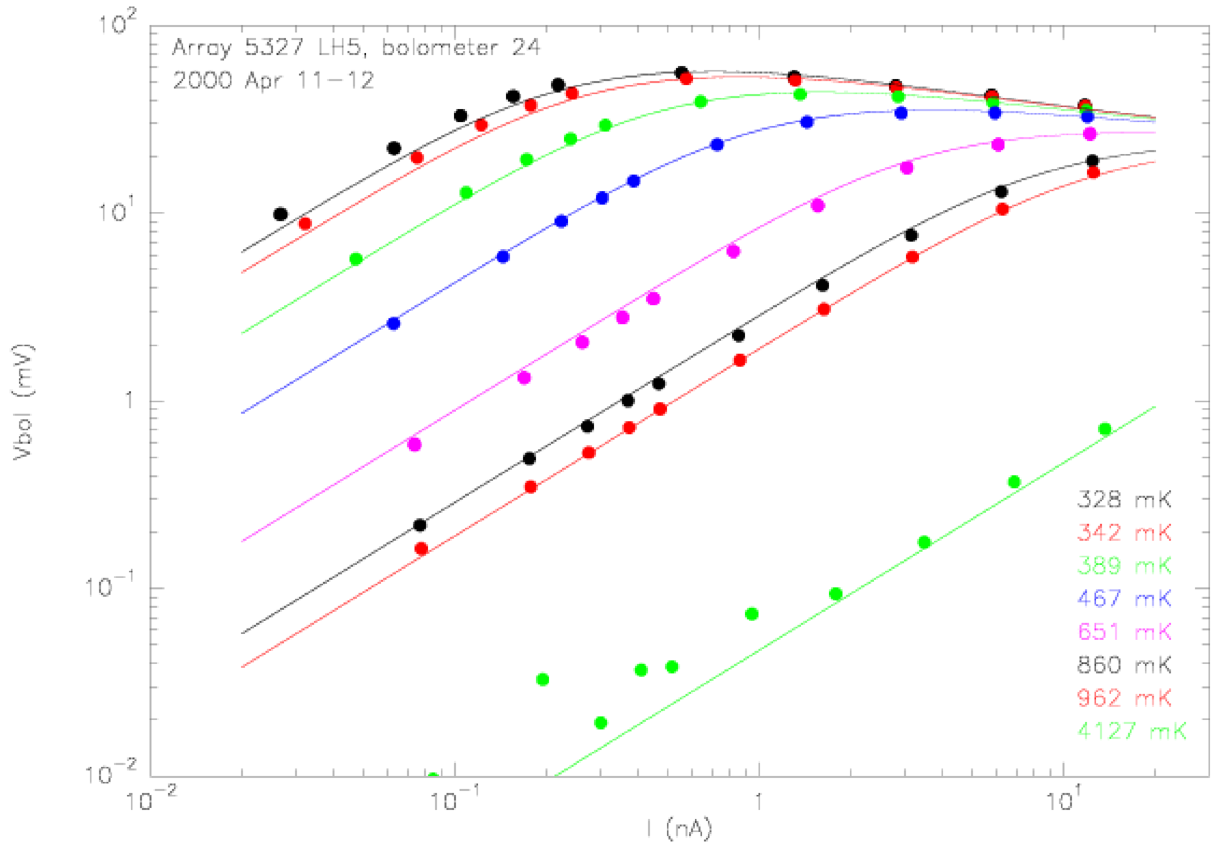

Figure 12. IV curves for a bolometer at multiple temperatures. The filled circles are measured data, and the lines are model fits with 4 free parameters.

The bolometer parameters are derived from a minimization procedure in which the measured I's and V's are compared with a best-fit four-parameter model. The model is:

- $R = R_0 \exp[(T_0/T)^{1/2}]$
- $G = G_0\, T^{beta}$

See Mather (1982) for further details of the model.

```
G0 test array 5327 LH5
Data at 328, 342, 389, 467, 651, 860, 962, 4127 mK
Negative data included; 4127 mK duplicated
Updated 1 May 2000, 16:30 PDT

R = R0 exp(sqrt(T0/T))
G = G0 T^beta
```

bol/grp	R0 ohms	T0 K	R* 0.3 K Mohms	R 0.5 K Mohms	G0=G(1 K) W/K^(beta+1)	beta	G(0.3 K)* W/K	G(0.5 K) W/K
17 HG2D	1195	51.45	582	30.4	62.3 e-9	2.85	2.02 e-9	8.64 e-9
18 HG2D	1222	51.62	608	31.6	61.9 e-9	2.84	2.03 e-9	8.65 e-9
19 HG2D	1289	50.52	557	29.9	59.0 e-9	2.70	2.29 e-9	9.08 e-9
20 HG2C	1481	48.99	525	29.5	1.56e-9	1.18	0.38 e-9	0.69 e-9

21	HG2C	1321	50.76	589	31.4	1.66e-9	1.31	0.34 e-9	0.67 e-9
22	HG2C	1316	50.67	580	31.0	1.68e-9	1.31	0.35 e-9	0.68 e-9
23	HG2B	1412	49.70	549	30.2	1.61e-9	1.25	0.36 e-9	0.68 e-9
24	HG2B	1474	49.36	549	30.4	1.57e-9	1.23	0.36 e-9	0.67 e-9
25	HG2B	1363	50.43	582	31.3	1.62e-9	1.30	0.34 e-9	0.66 e-9
26	HG2A	1277	51.60	634	33.0	59.9 e-9	2.81	2.03 e-9	8.54 e-9
27	HG2A	1358	51.20	640	33.7	57.5 e-9	2.74	2.12 e-9	8.61 e-9
28	HG2A	1336	50.88	605	32.1	58.8 e-9	2.71	2.25 e-9	8.99 e-9
29	HG1A	1290	51.96	670	34.5	24.2 e-9	2.63	1.02 e-9	3.91 e-9
32	mem.	1299	51.76	658	34.1	202 e-9	2.31	12.5 e-9	40.7 e-9

* extrapolation

Table 7. Four-parameter fits for G_0 bolometer array 5327 LH5.

The fits in Table 7 are somewhat unsatisfactory, as evidenced by the systematic underestimate of the bolometer resistance at the lowest and highest temperatures (Figure 12). Better fits are obtained with a slightly different thermistor behavior, such as $R = R_0 \exp[(T_0/T)^{0.59}]$. Alternatively, we fit just the data at the colder temperatures to achieve better accuracy there.

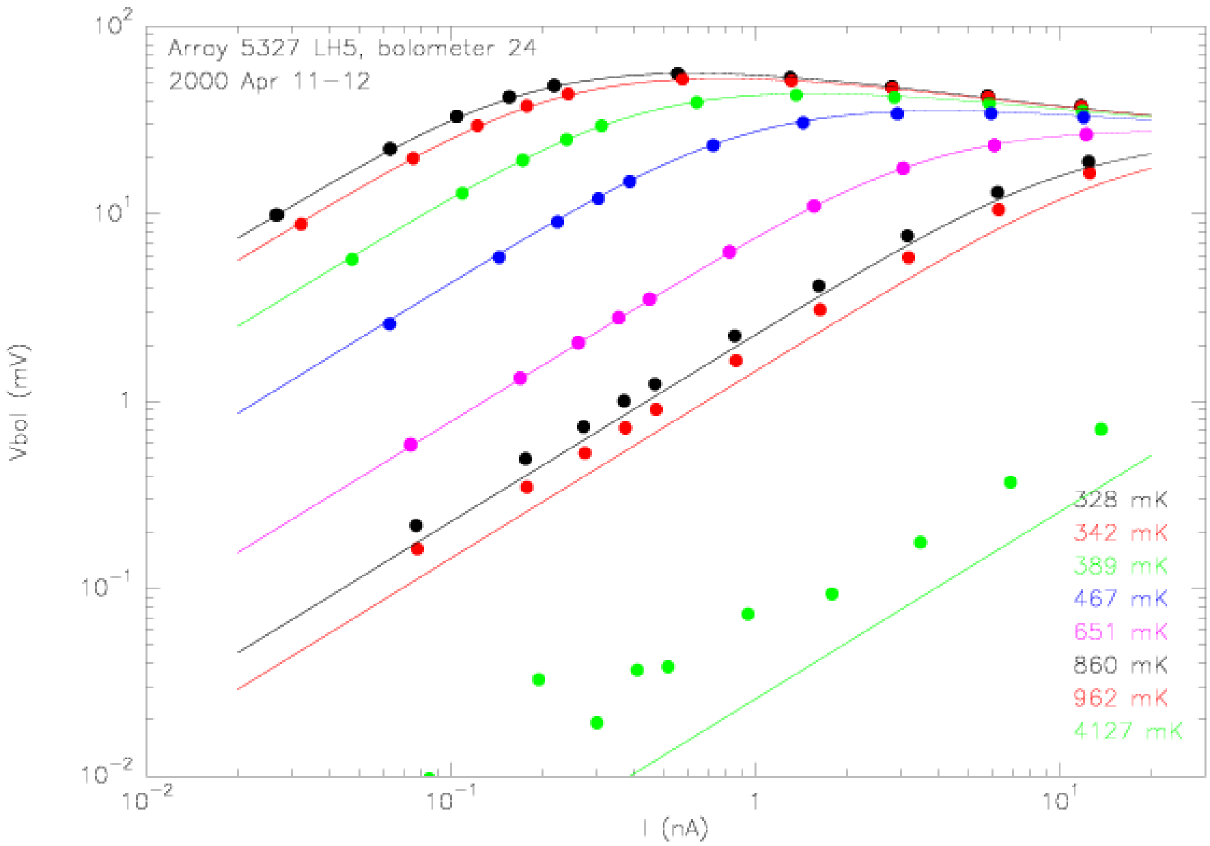

Figure 13. IV curves for bolometer 24, with fit to low temperature data only (T < 0.8 K).

```
G0 test array 5327 LH5
Data at 328, 342, 389, 467, 651 mK
```

Updated 1 May 2000, 16:40 PDT

R = R0 exp(sqrt(T0/T))
G = G0 T^beta

bol/grp	R0 ohms	T0 K	R* 0.3 K Mohms	R 0.5 K Mohms	G0=G(1 K) W/K^(beta+1)	beta	G(0.3 K)* W/K	G(0.5 K) W/K
17 HG2D	599	58.28	677	29.3	123 e-9	3.63	1.56 e-9	9.93 e-9
18 HG2D	539	59.68	720	29.9	135 e-9	3.72	1.53 e-9	10.2 e-9
19 HG2D	590	58.26	665	28.8	129 e-9	3.61	1.67 e-9	10.6 e-9
20 HG2C	581	58.39	665	28.7	2.44e-9	1.72	0.31 e-9	0.74 e-9
21 HG2C	580	59.08	721	30.5	2.46e-9	1.78	0.29 e-9	0.72 e-9
22 HG2C	589	58.76	705	30.1	2.47e-9	1.76	0.30 e-9	0.73 e-9
23 HG2B	587	58.51	682	29.3	2.45e-9	1.76	0.29 e-9	0.72 e-9
24 HG2B	597	58.46	689	29.6	2.41e-9	1.75	0.29 e-9	0.72 e-9
25 HG2B	596	58.78	715	30.5	2.40e-9	1.77	0.28 e-9	0.70 e-9
26 HG2A	632	58.62	744	31.9	118 e-9	3.60	1.55 e-9	9.73 e-9
27 HG2A	636	58.80	765	32.6	120 e-9	3.60	1.57 e-9	9.90 e-9
28 HG2A	627	58.44	722	31.1	124 e-9	3.58	1.67 e-9	10.4 e-9
29 HG1A	630	59.22	796	33.6	42.6 e-9	3.30	0.80 e-9	4.33 e-9
32 mem.	650	58.62	765	32.8	610 e-9	3.54	8.60 e-9	52.4 e-9

* extrapolation

Table 8. Four-parameter fits for array 5327 LH5, using only data at T < 0.8 K.

The fits using only the low temperature data give 0.3 K resistances which are ~20% higher, 0.5 K resistances which are ~2% lower, 0.3 K G's which are ~25% lower, and 0.5 K G's which are ~15% highe

The derived values of beta are somewhat surprising. The devices with only silicon legs have measured beta's of 1.3 - 1.8, while beta's of 3 (the value expected for a dielectric) were measured in the 12 micron silicon bolometers (e.g., Wang et al. 1996). The speculation is that the thermal conductance is dominated by the heavily doped traces, which have a metallic beta of 1 (H. Moseley, private communication).

The devices with metal on the legs, on the other hand, have steep beta's of 2.7 - 3.6. While normal metals should give a beta of 1, the aluminum metallization is superconducting at these temperatures and may have a much more steep beta.

The addition of 100 micron wide metal to the strap has essentially no effect on the thermal conductance. A bolometer with the design HGUNIT.2D (metal) has the same G as HGUNIT.2A (no metal), and HGUNIT.2C (metal) has the same G as HGUNIT.2B (no metal).

Parameter Fits for 5347 G_0 Test Array LH1

All bolometers were wired with 30 Mohm nichrome load resistors from MSI. The nicrohme resistors are much more temperature stable, and their resistance is known to 1% accuracy. The full array was measured with two separate cooldowns between which the routing of the 16 JFETs was changed.

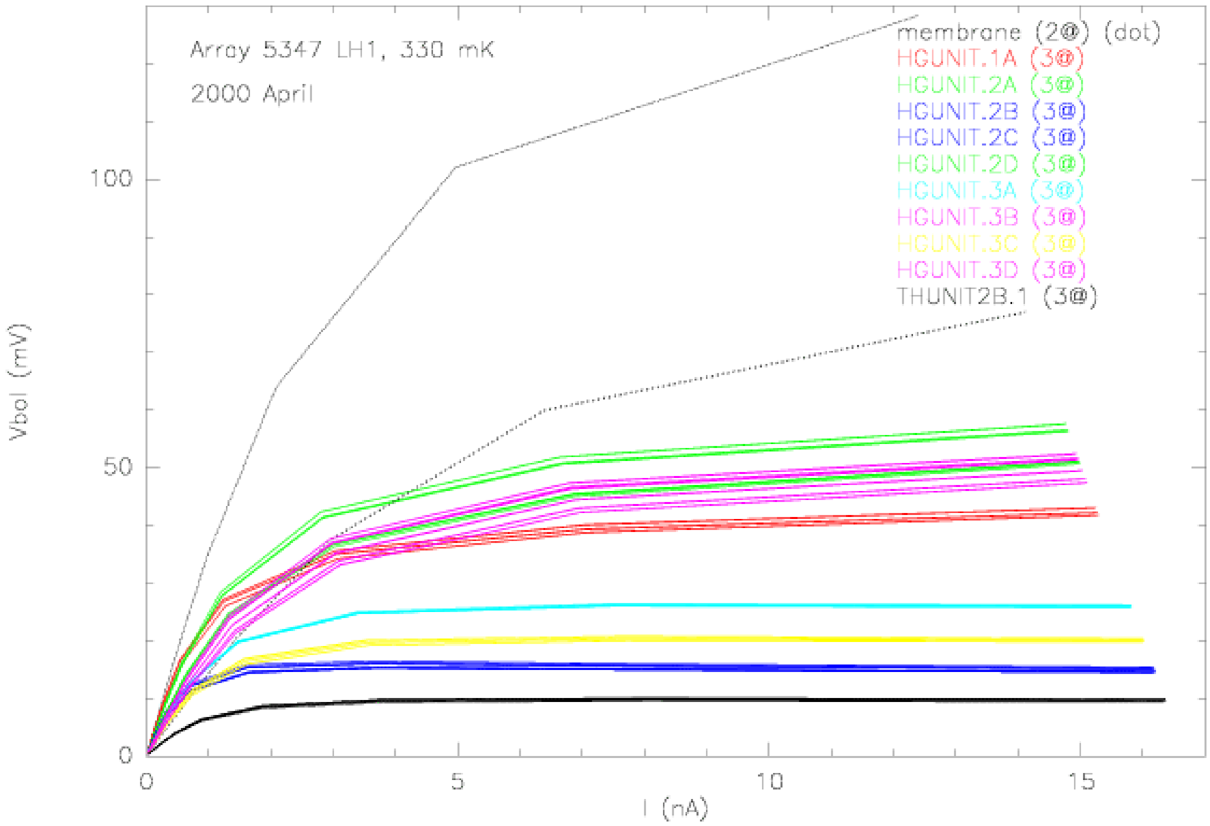

Figure 14. Sample IV curves for all bolometers at a single temperature.

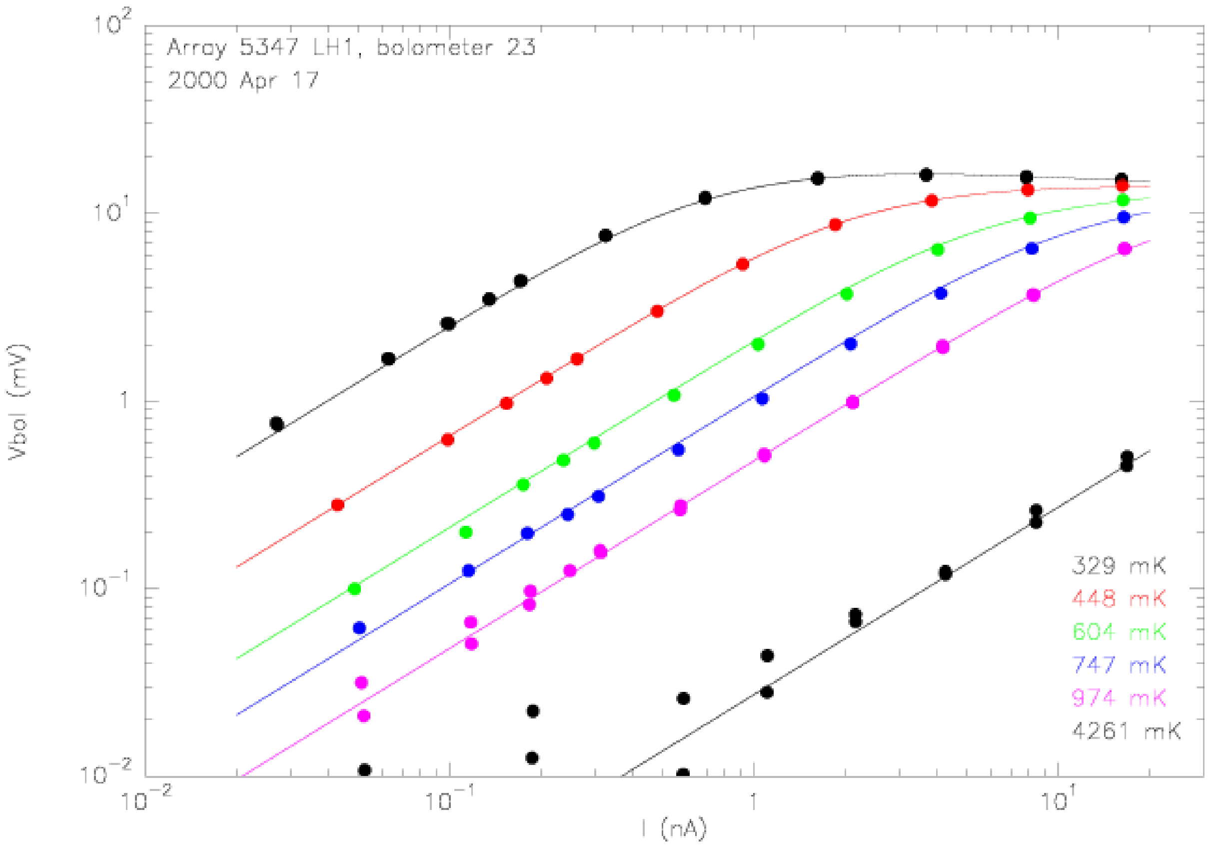

Figure 15. Sample IV curves for a single bolometer at multiple temperatures.

G0 test array 5347 LH1
Data at 330, 440, 597, 742, 985, 4243 mK (pixels 1-16)
Data at 329, 448, 604, 744, 974, 4261 mK (pixels 17-32)
Updated 1 May 2000, 16:50 PDT

R = R0 exp(sqrt(T0/T))
G = G0 T^beta

bol/grp	R0 ohms	T0 K	R* 0.3 K Mohms	R 0.5 K Mohms	G0=G(1 K) W/K^(beta+1)	beta	G(0.3 K)* W/K	G(0.5 K) W/K
01 mem.	1844	26.25	21.3	2.59	23.3 e-9	0.55	12.1 e-9	15.9 e-9
02 TH.1	1290	25.58	13.2	1.65	1.07e-9	1.32	0.22 e-9	0.43 e-9
03 TH.1	1365	25.51	13.8	1.73	1.20e-9	1.19	0.29 e-9	0.53 e-9
04 TH.1	1401	25.31	13.7	1.72	0.94e-9	1.15	0.24 e-9	0.42 e-9
05 HG3D	1953	26.94	25.5	3.01	24.4 e-9	1.97	2.28 e-9	6.23 e-9
06 HG3D	1956	27.16	26.5	3.11	24.1 e-9	1.96	2.28 e-9	6.19 e-9
07 HG3D	2147	27.11	28.9	3.39	19.4 e-9	1.77	2.30 e-9	5.69 e-9
08 HG3C	2127	26.93	27.7	3.27	2.24e-9	1.20	0.53 e-9	0.98 e-9
09 HG3C	1844	27.58	26.9	3.10	2.66e-9	1.38	0.51 e-9	1.02 e-9
10 HG3C	1898	27.05	25.2	2.97	2.61e-9	1.35	0.51 e-9	1.02 e-9
11 HG3B	1934	28.40	32.5	3.63	24.2 e-9	2.03	2.10 e-9	5.93 e-9
12 HG3B	1908	28.51	32.7	3.63	25.1 e-9	2.06	2.10 e-9	6.02 e-9
13 HG3B	1869	28.76	33.4	3.68	27.8 e-9	2.14	2.11 e-9	6.31 e-9
14 HG3A	1840	28.67	32.4	3.58	4.08e-9	1.44	0.72 e-9	1.50 e-9
15 HG3A	1951	28.41	32.9	3.66	3.80e-9	1.42	0.69 e-9	1.42 e-9
16 HG3A	1924	28.37	32.2	3.59	3.89e-9	1.41	0.71 e-9	1.46 e-9

17	HG2D	1893	28.73	33.7	3.71	38.4 e-9	2.63	1.62 e-9	6.20 e-9
18	HG2D	1899	28.90	34.8	3.80	38.7 e-9	2.66	1.57 e-9	6.12 e-9
19	HG2D	1981	28.82	35.8	3.93	36.7 e-9	2.65	1.51 e-9	5.85 e-9
20	HG2C	2025	28.51	34.7	3.85	1.17e-9	1.35	0.23 e-9	0.46 e-9
21	HG2C	1839	28.97	34.1	3.72	1.31e-9	1.43	0.23 e-9	0.49 e-9
22	HG2C	1920	28.91	35.2	3.85	1.26e-9	1.40	0.23 e-9	0.48 e-9
23	HG2B	1957	29.47	39.4	4.22	1.21e-9	1.37	0.23 e-9	0.47 e-9
24	HG2B	2038	29.15	38.9	4.22	1.17e-9	1.34	0.23 e-9	0.46 e-9
25	HG2B	1929	29.84	41.4	4.37	1.25e-9	1.40	0.23 e-9	0.47 e-9
26	HG2A	1871	30.40	44.0	4.55	42.4 e-9	2.76	1.53 e-9	6.26 e-9
27	HG2A	2019	29.93	44.0	4.63	37.3 e-9	2.62	1.59 e-9	6.07 e-9
28	HG2A	1952	30.41	46.0	4.76	40.0 e-9	2.69	1.57 e-9	6.20 e-9
29	HG1A	1836	31.16	49.0	4.92	20.0 e-9	2.74	0.74 e-9	2.99 e-9
30	HG1A	1788	31.95	54.2	5.30	20.7 e-9	2.80	0.71 e-9	2.97 e-9
31	HG1A	1927	31.34	52.9	5.29	18.1 e-9	2.68	0.72 e-9	2.82 e-9
32	mem.	1814	32.12	56.5	5.49	72.9 e-9	1.58	10.9 e-9	24.4 e-9

* extrapolation

Table 9. Four-parameter fits for G_0 bolometer array 5347 LH1.

Although the measured values of G make qualitative sense, the scaling with leg geometry is not what was expected. This will be discussed further in the Conclusions.

Resistance Gradient

The cold resistance goes from high at bolometer 32 to low at bolometer 1. In order to confirm this situation, a few bolometers were measured individually with an electrometer. The 0.327 K resistance measured in the linear portion of the IV curve is tabluated below:

Bolometer	Electrometer Resistance Mohm	Table 9 Fit Resistance Mohm
1	15.6	14.4
9	19	18.0
12	23	21.7
15	22	21.8
24	28	25.7
32	36.4	36.6

Table 10. Resistance gradient in G_0 array 5347 LH1.

A radiation gradient as the cause of the resistance can be ruled out since the membrane (high G) devices and bolometers (low G) are affected about the same. WHAT ABOUT A TEMPERATURE GRADIENT???

Noise for 5347 G_0 Test Array LH1

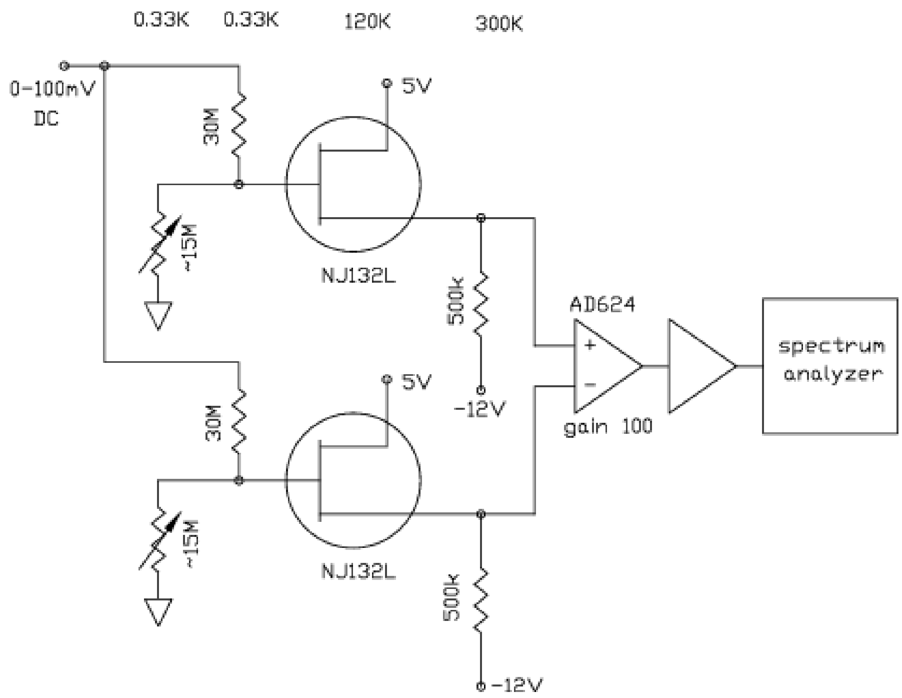

Figure 16. Differential readout used for noise measurements. The differential readout was the only one available with the desired bandwidth (lowpass filtering at ~250 Hz), but it has the advantage of common mode noise rejection of bias fluctuations and microphonics.

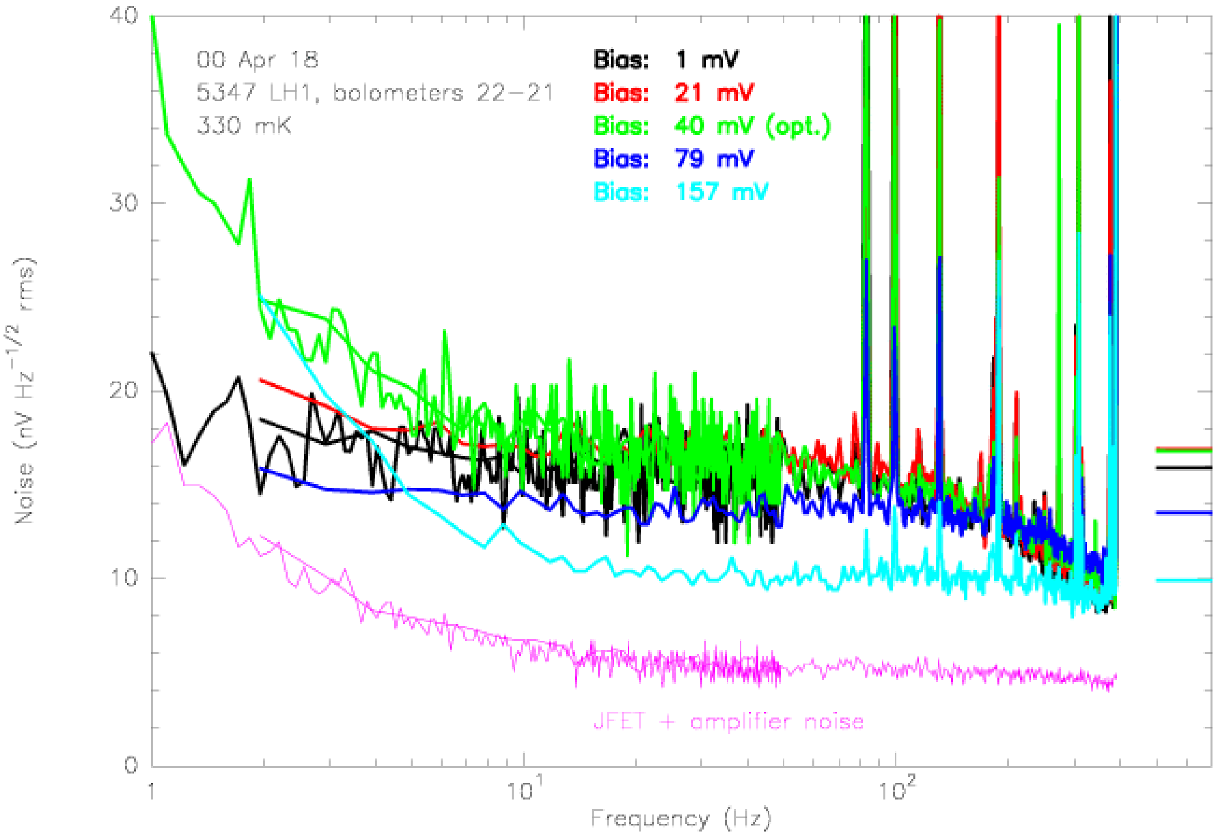

Figure 17. Noise spectra for bolometers 22-21 on 5347 G_0 array LH1. The bolometers are of type HGUNIT2C. The observed noise has been divided by the amplifier gain (except the low pass filtering) and by $2^{1/2}$ to show the noise for a single bolometer referred to the JFET input. The 1/f noise in the 40 mV and 157 mV spectra is most likely due to operation of the JFETs at a non-optimal temperature. The short horizontal lines at right show the noise predicted from the IV curve fits in the ~30 Hz region. The predictions are in good agreement with the observations. The calculated electrical NEP for the optimal 40 mV bias is 6.1×10^{-17} W $s^{1/2}$.

Time Constants for 5347 G_0 Test Array LH1

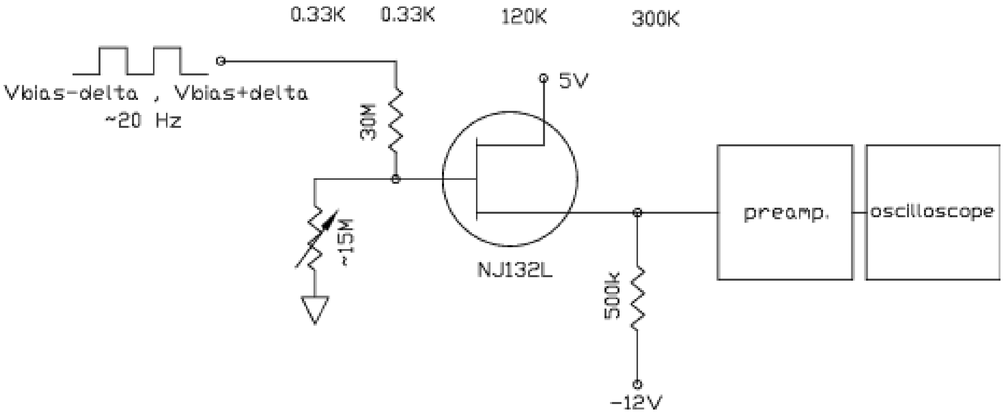

Figure 18. Circuit used for time constant measurements.

For the time constant measurements, the bolometers were driven using a bias waveform with a square profile switching between two positive levels 8 mV apart. The output of the JFET was sent to an SR560 preamplifier with a gain of 100 and then to an oscilloscope. DC coupling was used on both instruments; a DC level from a power supply was subtracted to bring the signal on scale. Low-pass filtering was applied with the SR560, but the cutoff frequency (typically 3 kHz) was chosen so that only high frequency noise was eliminated and the shape of the waveform was preserved.

Additional filtering of the bolometer waveform was caused by the bias waveform filtering (cutoff frequency at 6800 Hz) and the RFI connectors (cutoff frequency at 20 kHz, assuming a 1000 ohm JFET output impedance). These cutoff frequencies are high enough to be irrelevant.

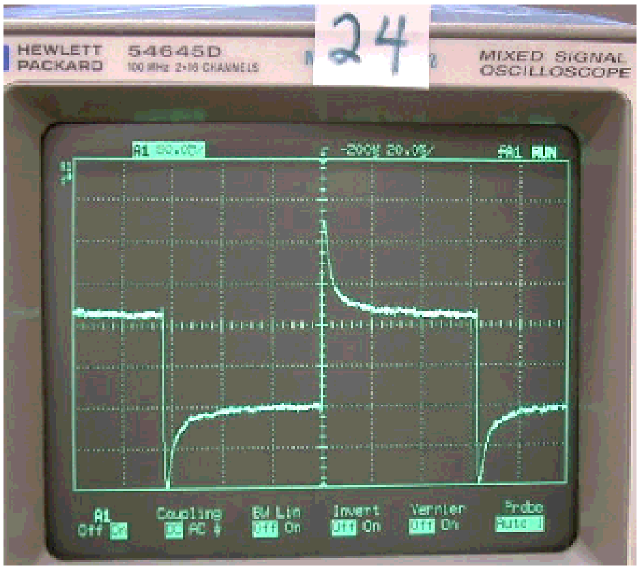

Figure 19. Typical oscilloscope trace during time constant measurement. Shown is the output of the JFET for bolometer 24 of the 5347 G_0 test array, multiplied by a gain of 100. The bias frequency was 8 Hz, and the settling time was 3.6 msec.

The overshoot is caused by the high-frequency impedance of the bolometer being larger than the low-frequency impedance (Mather 1982). Stated another way, the dynamic circuit model of a bolometer contains an effective inductance, which creates a voltage spike at the transition of the bias. Our interpretation is that the settling time of the voltage following the bias transition is the true detector time constant (tau_e in the notation of Mather 1982).

For the measured quantities, we looked at the transition caused by the positive change in the bias. We recorded:

- V(step) -- the voltage from the initial (flat) voltage to the final (flat) voltage.
- V(o.s.) -- the voltage from the final (flat) voltage to the peak voltage. ('o.s.' for overshoot.)
- t(o.s.) -- the time from the beginning of the transition to the peak voltage.
- t(settle) -- the time from the peak to when the voltage has slewed 63% of the way to the final voltage. The true time constant tau_e.

In the table below, voltages are referred to JFET output, before the preamplification. The calculated G and T are the estimates from the IV curve fits.

bol.	grp.	bias mV	calc G nw/K	calc T K	V(o.s.) mV	t(o.s.) msec	calc. V(step) mV	observ. V(step) mV	t(settle) msec
9	3C	25	0.59	0.34	0.12	2.2	2.9	2.7	1.5
9	3C	49*	0.64	0.36	0.42	1.1	1.4	1.4	1.6
9	3C	98	0.76	0.40	0.70	0.52	0.34	0.40	1.2
9	3C	196	0.98	0.48	0.61	0.28	0.02	0.06	0.71
15	3A	39	0.84	0.34	0.19	1.8	2.2	2.2	1.6
15	3A	78?*	0.95	0.38	2.8?	0.92	0.90	6.6?	1.1
15	3A	157	1.20	0.44	0.69	0.31	0.12	0.18	0.61
15	3A	314	1.60	0.54	0.47	0.24	-0.02	0.05	0.31
18	2D	49	2.1	0.34	N.A.	N.A.	2.7	2.6	0.38
18	2D	98*	2.5	0.36	0.20	0.8	1.5	1.5	0.68
18	2D	196	3.6	0.41	0.46	0.31	0.45	0.53	0.36
18	2D	392	5.6	0.48	0.34	0.22	0.12	0.22	0.16
24	2B	20	0.28	0.34	0.39	2.4	2.6	2.7	4.5
24	2B	39*	0.31	0.37	1.1	1.3	1.2	1.1	3.6
24	2B	78	0.38	0.43	1.2	0.6	0.17	0.11	2.3
24	2B	157	0.50	0.53	0.74	0.4	-0.03	-0.13	1.3

* optimum bias for NEP
? apparent errors in measurement, probably bias amplitude setting

Table 11. Time constant measurements for G_0 array 5347 LH1 operated at 0.328 K.

Results for 5347 Thermistor Test Array RH7

Fitted Parameters

```
Thermistor test array 5347 RH7
Data at 330, 451, 610, 755, 971, 4190 mK
Updated 1 May 2000, 16:55 PDT
```

R = R0 exp(sqrt(T0/T))
G = G0 T^beta

bol/grp	R0 ohms	T0 K	R* 0.3 K Mohms	R 0.5 K Mohms	G0=G(1 K) W/K^(beta+1)	beta	G(0.3 K)* W/K	G(0.5 K) W/K
09 TH.1	1622	35.93	91.8	7.79	1.53e-9	1.67	0.20 e-9	0.48 e-9
10 TH.1	1658	35.50	87.9	7.57	1.52e-9	1.64	0.21 e-9	0.49 e-9
11 TH.1	1622	35.65	88.0	7.54	1.54e-9	1.69	0.20 e-9	0.48 e-9
12 TH.2	1800	34.29	79.1	7.11	1.42e-9	1.49	0.24 e-9	0.51 e-9
13 TH.2	1733	34.60	80.0	7.10	1.48e-9	1.53	0.23 e-9	0.51 e-9
14 TH.2	1726	34.57	79.3	7.05	1.49e-9	1.52	0.24 e-9	0.52 e-9
15 TH.2	1800	34.52	82.0	7.31	1.44e-9	1.51	0.23 e-9	0.51 e-9
16 TH.2	1802	34.41	80.7	7.22	1.44e-9	1.50	0.24 e-9	0.51 e-9
17 TH.3	1638	36.36	99.0	8.28	1.50e-9	1.57	0.23 e-9	0.51 e-9
18 TH.3	1668	36.19	98.2	8.26	1.49e-9	1.56	0.23 e-9	0.51 e-9
19 TH.3	1727	36.17	101	8.53	1.43e-9	1.56	0.22 e-9	0.48 e-9
20 TH.3	1693	36.09	98.2	8.29	1.46e-9	1.56	0.22 e-9	0.50 e-9
21 TH.3	1578	36.79	102	8.38	1.55e-9	1.62	0.22 e-9	0.50 e-9
22 TH.4	1096	33.11	40.0	3.75	1.42e-9	1.45	0.25 e-9	0.52 e-9
23 TH.4	1106	33.47	42.8	3.95	1.37e-9	1.42	0.25 e-9	0.51 e-9
24 TH.4	1108	33.03	40.0	3.75	1.37e-9	1.42	0.25 e-9	0.51 e-9

* extrapolation

Table 12. Four-parameter fits for thermistor test array 5347 RH7.

There is no strong resistance gradient across the RH7 thermistor device, as confirmed by the following 0.330 K measurements with an electrometer:

Bolometer	Electrometer Resistance Mohm
1	42.8
6	44
31	44
32	35.0

Table 13. Electrometer resistance measurements for thermistor test array 5347 RH7.

Noise -- DC Bias

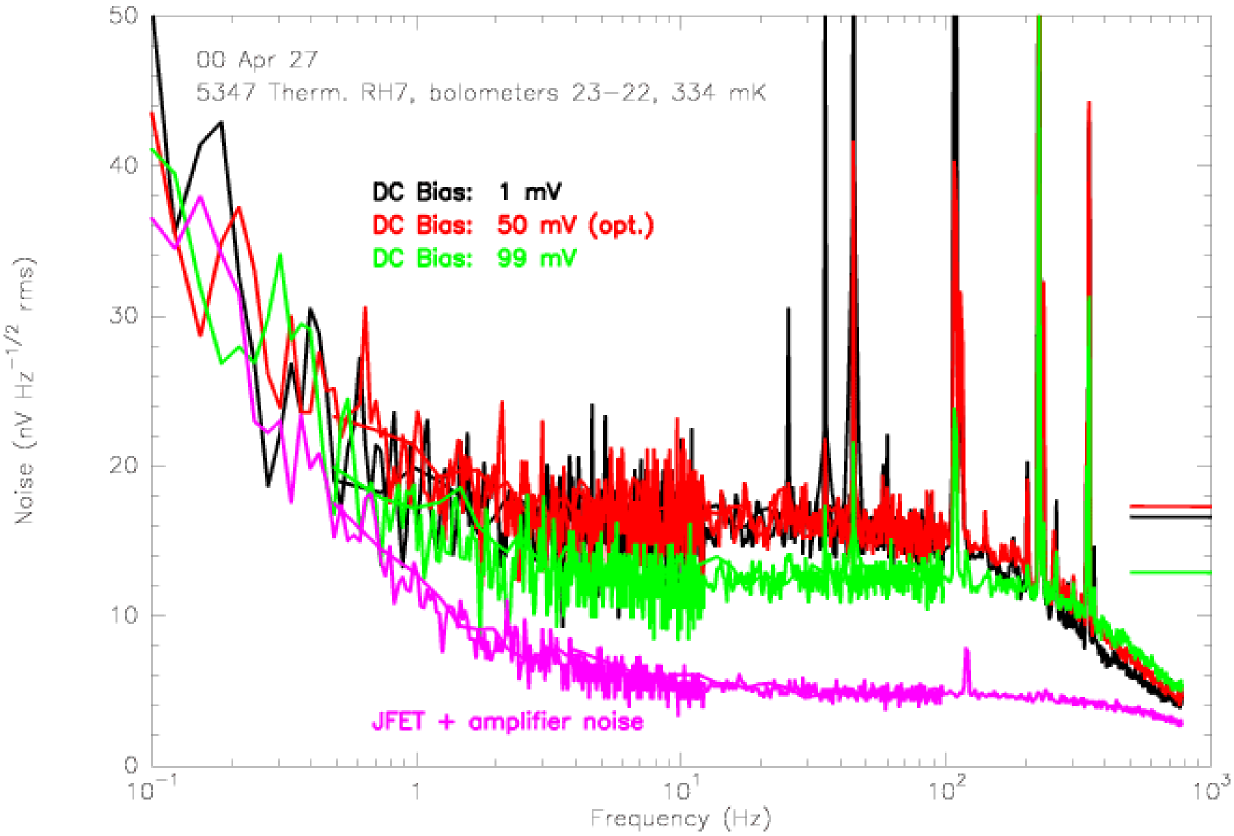

Figure 20. Noise spectra for bolometers 23-22 on 5347 thermistor test array RH7. The measurement technique and analysis are the same as in Figures 16 and 17. The bolometers are of type THUNIT2B.1 and have full-area thermistors. The predictions at right are for 10 Hz.

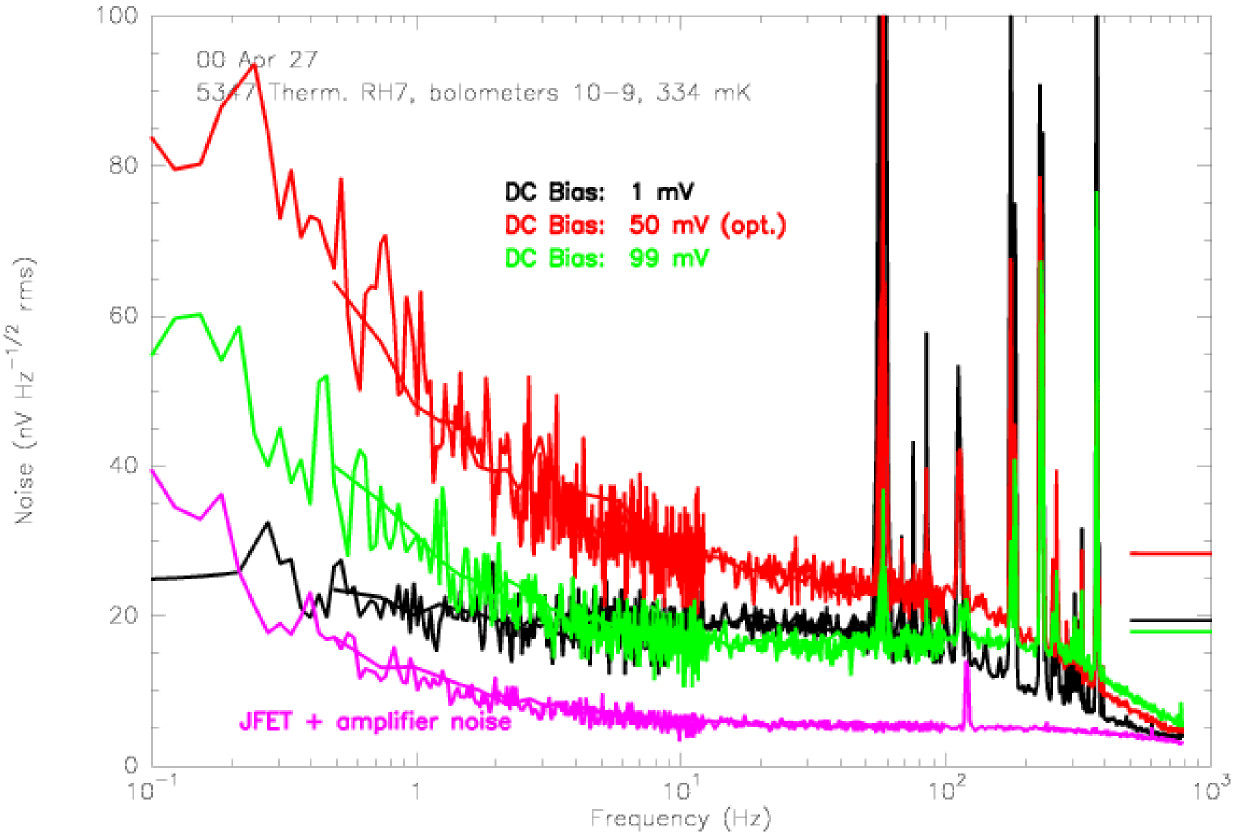

Figure 21. Noise spectra for bolometers 10-9 on 5347 thermistor test array RH7. The bolometers are of type THUNIT2B.4 and have small thermistors. The veritical display range has been enlarged by a factor of 2 compared to Figure 20.

Low Frequency Noise (AC Bias)

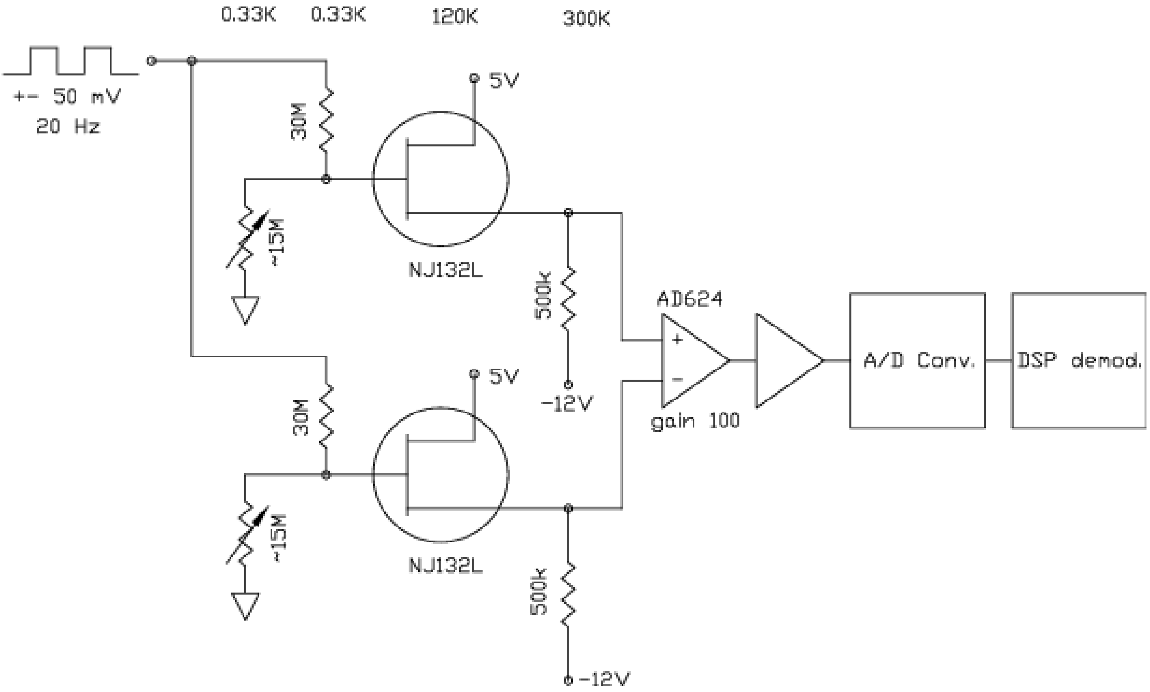

Figure 22. Electronics configuration used to measure low-frequency noise. The amplifier circuit is the same as in Figure 16. Differences now are the AC bias on the detector and demodulation (in the DSP) prior to the Fourier transform (in software).

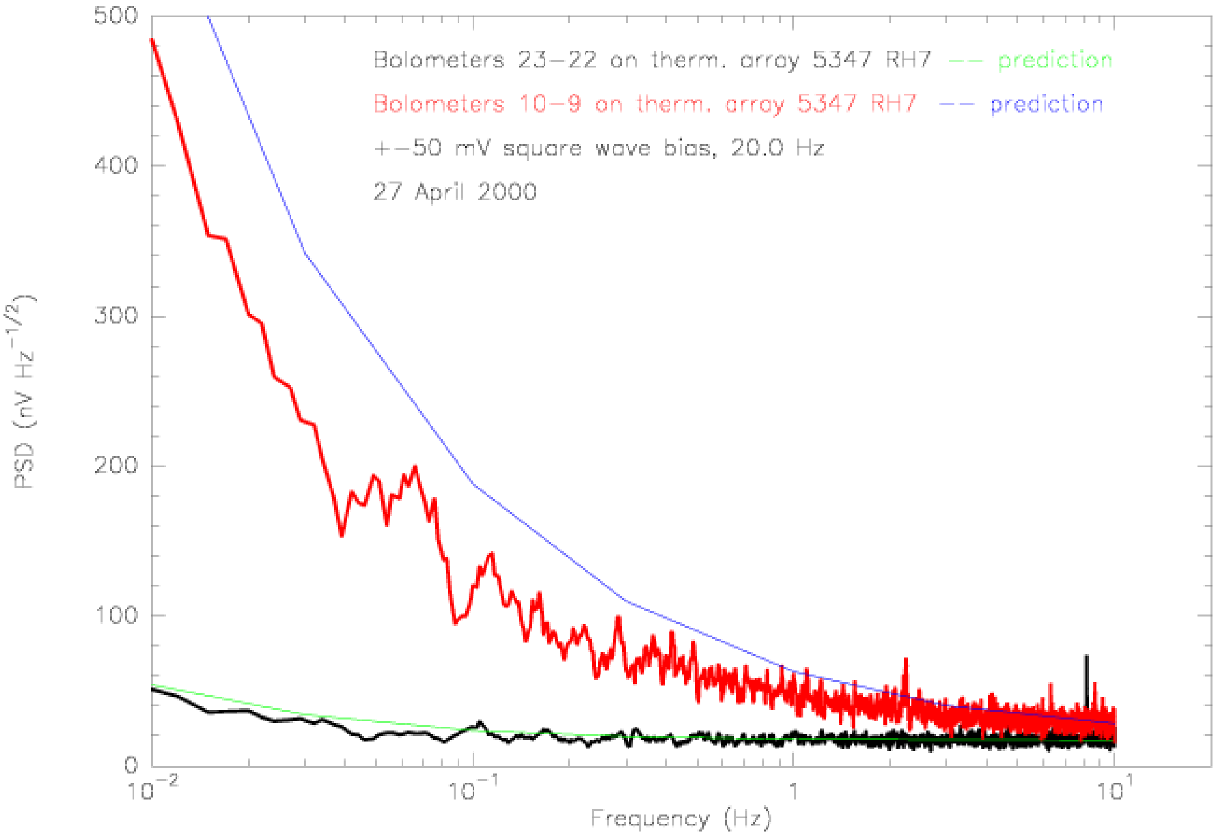

Figure 23. Low-frequency noise spectra for bolometers 23-22 and 10-9 on 5347 thermistor test array RH7. The noise has been divided by $2^{1/2}$ and corrected for the amplifier gain to express the noise for a single bolometer. The predictions are based on the IV curves and the 1/f noise model of Han et al. (1998). For the bolometers with full-area thermistors, an NEP of 2×10^{-16} W $s^{1/2}$ was observed at 0.01 Hz, and 9×10^{-17} W $s^{1/2}$ at 0.1 Hz.

Time Constants

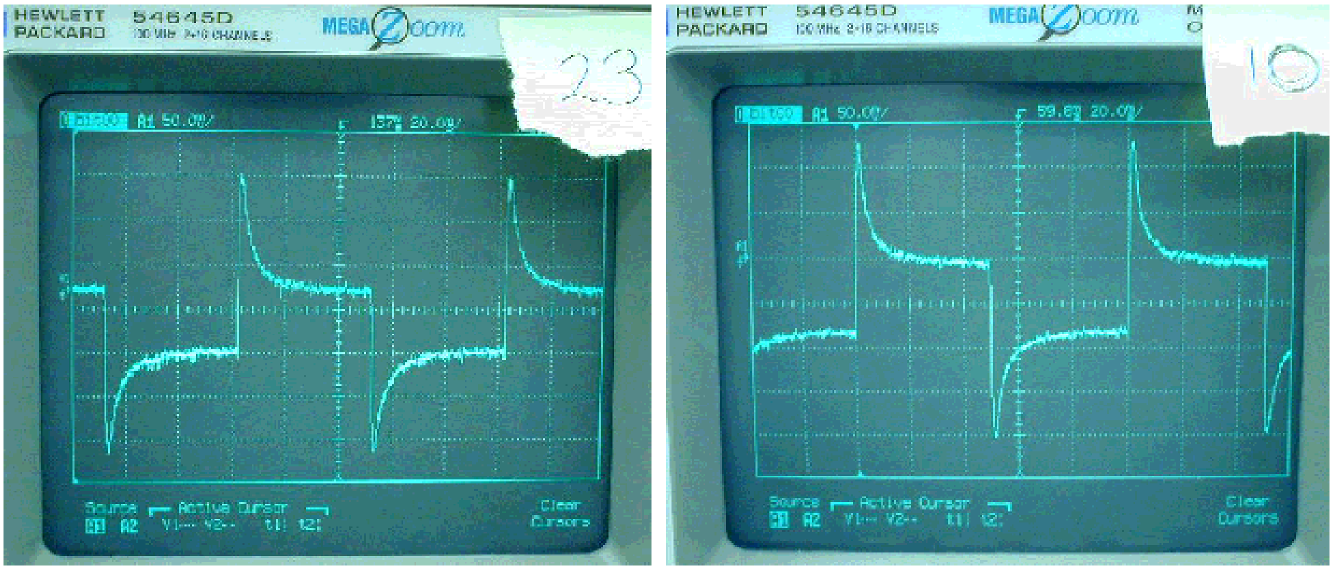

Figure 24. Oscilloscope traces during time constant measurements of bolometers 23 (full area thermistor) and 10 (small thermistor) from thermistor test array 5347 RH7. The measurement technique was the same as in Figure 19. The bias frequency was 10 Hz. The transition times are similar.

bol.	grp.	bias mV	calc G nw/K	calc T K	V(o.s.) mV	t(o.s.) msec	calc. V(step) mV	observ. V(step) mV	t(settle) msec
10	2B.4	50*	0.34	0.40	1.3	1.3	0.82	0.80	3.6
10	2B.4	100	0.47	0.49	1.1	0.36	-0.044	-0.025	2.1
23	2B.1	50*	0.36	0.39	1.3	1.2	0.73	0.70	4.2
23	2B.1	100	0.45	0.46	1.1	0.58	0.035	0.019	2.8

* optimum bias for NEP

Table 14. Time constant measurements for thermistor test array 5347 RH7 operated at 0.331 K.

At these temperatures, the size of the thermistor only plays a small role in the time constant and heat capacity -- 30% at most.

General Conclusions

The following conclusions apply to the operating temperatures of the measurements (0.33 - 1 K):

1. Doping of ND = 0.75+-0.05 is suitable for HAWC and SHARCII. However, an accurate selection of doping is made difficult by the resistance variation across the 5347 (ND = 0.75) wafer.
2. The 5327 (ND = 0.70) wafer had 0.3 K resistances of ~480 Mohms/square and 0.5 K resistances of ~22 Mohms/square.
3. The 5347 (ND = 0.75) wafer had 0.3 K resistances of ~32 Mohms/square, but with a range of 9.7 to 70. The 0.5 K resistances were ~3.1 Mohms/square, with a range of 1.4 to 5.9.
4. Bolometers with no metal on the torsion bars have thermal conductances with a $T^{1.2}$ to $T^{1.8}$ temperature dependence.
5. Adding aluminum to the torsion bars significantly increases the thermal conductances and changes

the temperature dependence to $T^{2.0}$ to $T^{3.6}$.

6. Adding metal to the strap region has a minimal effect on the thermal conductance.
7. The quantitative behavior of the thermal conductances is discussed below.
8. The electrical time constants for the detectors at 0.4 K are approximately 1 msec for a G of 1 nW/K.
9. The heat capacity from large thermistors is not significant compared to the rest of the pixel. The contribution of a full area thermistor is ~25% at 0.4 K.
10. There is no evidence for excess noise in the bolometers in the white noise region (a few Hz to ~100 Hz). Electrical NEP's down to 6×10^{-17} W $s^{1/2}$ have been observed.
11. With a full-area thermistor, the useful bolometer signal band can be extended down to ~10 mHz, permitting scanning observing modes. The 1/f noise roughly follows the prediction of Han et al. (1998).

The most perplexing aspect of the detector measurements is the behavior of the thermal conductances, summarized in the table below:

therm. struct.	wafer/sample	tors. bar silicon W/L	tors. bar metal W/L	G(0.3 K)* nW/K	G(0.5 K) nW/K
HG2B, HG2C, TH2B	5327 G0 LH5	0.038	0	0.28- 0.38	0.66- 0.74
HG2B, HG2C, TH2B	5347 G0 LH1	0.038	0	0.22- 0.29	0.42- 0.53
HG2B, HG2C, TH2B	5347 th RH7	0.038	0	0.20- 0.25	0.48- 0.52
HG3C	5347 G0 LH1	0.068	0	0.51- 0.53	0.98- 1.02
HG3A	5347 G0 LH1	0.068	0.136^	0.69- 0.72	1.41- 1.50
HG1A	5327 G0 LH5	0.022	0.022	0.80- 1.02	3.91- 4.33
HG1A	5347 G0 LH1	0.022	0.022	0.71- 0.74	2.82- 2.99
HG2A, HG2D	5327 G0 LH5	0.038	0.038	1.53- 2.29	8.54-10.6
HG2A, HG2D	5347 G0 LH1	0.038	0.038	1.51- 1.62	5.85- 6.26
HG3B, HG3D	5347 G0 LH1	0.068	0.068	2.10- 2.30	5.69- 6.31
membrane	5327 G0 LH5	large	large	8.60-12.5	40.7 -52.4
membrane	5347 G0 LH1	large	large	10.9	24.4

* extrapolation
^ only on cold half of torsion bar

Table 15. Summary of thermal properties of HGUNIT's and THUNIT's.

As noted in the section "Results for 5327 G_0 Test Array LH5", the G's for metal-free legs go as ~$T^{1.5}$, and the G's for the metallized legs go as ~T^2. We have offered an explanation for the unexpected temperature dependence in that section.

The HGUNIT.2B/C, HGUNIT.3C, and HGUNIT.3A devices on 5347 G0 array LH1 can be used to estimate the dependence of G on torsion bar width and length for devices with no metal; we calculate a $W^{1.06}L^{-0.45}$ dependence at 0.3 K and $W^{1.03}L^{-0.53}$ at 0.5 K. (We have assumed that the metal half-way up the torsion bar on HGUNIT.3A is sufficient to cool that part of the bar to the base operating temperature.) In macroscopic/high temperature situations, we expect W^1 and L^{-1}, so the observed L dependence is surprising.

For the metallized devices (HGUNIT.1A, HGUNIT.2A/D, and HGUNIT.3B/D), the situation is even more surprising. The range of torsion bar lengths is not large, so we fit for the dependence of G on (W/L) together and calculate $(W/L)^{0.99}$ at 0.3 K and $(W/L)^{0.64}$ at 0.5 K, dominated presumably by width dependence. This is quite far from the expected $(W/L)^2$ dependence. It is possible that the 0.5 K measurements of the metallized bolometers especially are contaminated by heating effects in the silicon frame and/or detector package.

Recommendation for SHARCII Bolometer Design

Following is the SHARCII bolometer design recommendation resulting from this study:

- Full area thermistor (>=900 micron by >=900 micron).
- Target resistance of 10 Mohms at 0.5 K. Acceptable range: 5-20 Mohms. This resistance will be achieved with ND ~ 0.73 and will result in T_0 ~ 40 K and R_0 ~ 1300 ohms/square.
- Thermal design intermediate between HGUNIT.2B and HGUNIT.3C -- a torsion bar with W ~ 25 micron, L ~ 500 micron, and no metallization. HGUNIT.2B is also acceptable.

The following table summarizes the expected operating conditions of the SHARCII bolometers as designed above:

parameter	value	units
operating temperature	0.32	K
T0	40	K
R0	1300	ohm
thermistor volume	2.7e-7	cm^3
G0	1.9	W K^-2.35
beta (G = G0 T^beta)	1.35	
R (load resistor)	200	Mohm
T (load resistor)	2.0	K
background power	75	pW
NEP (background)	4.4e-16	W s^1/2
voltage noise (amp.)	5 e-9	V s^1/2
V (bias)	500	mV
V (bolometer)	19.4	mV
I	2.4	nA
R (bolometer)	8.1	Mohm
Z (bolometer)	2.8	Mohm
T (bolometer)	0.52	K
G	0.79	nW/K
S	1.3e+8	V/W
NEP (detector, 0.01 Hz)	2.8e-16	W s^1/2
NEP (detector, 0.1 Hz)	1.4e-16	W s^1/2
NEP (detector, 1 Hz)	1.2e-16	W s^1/2
NEP (detector, 10 Hz)	1.2e-16	W s^1/2
det. volt. noise, 10 Hz	16 e-9	V s^1/2
time constant (elec.)	1	msec

Table 16. SHARCII bolometer characteristics, updated from Moseley et al. (1999).

Recommendation for HAWC Bolometer Design

TBD

References

Han, S.-I., et al. 1998, in EUV, X-Ray, and Gamma-Ray Instrumentation for Astronomy IX, ed. O. Siegmund & M. Gummin, Proc. SPIE 3445, "Intrinsic 1/f Noise in Doped Silicon Thermistors for Cryogenic Calorimeters"

Locatelli, M., Arnaud, D., & Routin, M. 1976, *journal unknown*, "Thermal conductivity of some insulating materials below 1K"

Mather, J. C. 1982, Applied Optics 21, 1125, "Bolometer noise: nonequilibrium theory"

Moseley, H. 1999, memo dated July 29, "Detector Design for HAWC"

Moseley, S. H, Dowell, C. D., Allen, C, & Phillips, T. G. 1999, in Imaging at Radio Through Submillimeter Wavelengths, ed. J. Mangum & S. Radford, ASP Conf. Ser., "Semiconducting Pop-Up Bolometers for Far-Infrared and Submillimeter Astronomy"

Toloukian, Y. S., Powell, R. W., Ho, C. Y., & Klemens, P. G. 1970, Thermal Properties of Matter, Volume 1, Thermal Conductivity -- Metallic Elements and Alloys, IFI/Plenum: New York

Wang, N., et al. 1996, Applied Optics, 35, 6629, "Characterization of a submillimeter high-angular-resolution camera with a monolithic silicon bolometer array for the Caltech Submillimeter Observatory"